Journal of Materials Chemistry C

Accepted Manuscript

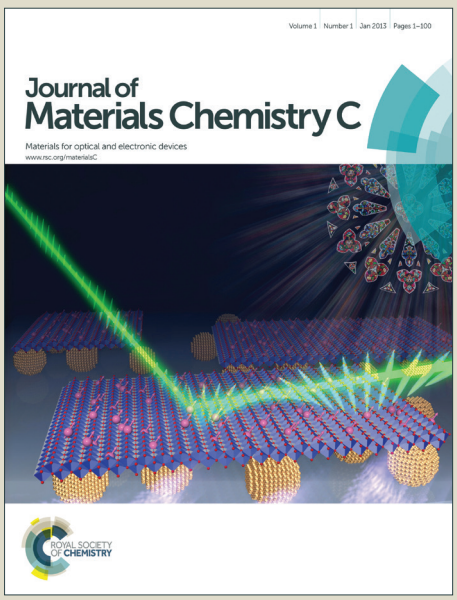

ROYAL SOCIETY OF CHEMISTRY

www.rsc.org/materialsC

Journal Name

ARTICLE TYPE

Cite this: DOI: 10.1039/xxxxxxxxxx

Comparison of local distortions in $Ba_8Ga_{16}X_{30}$ (X =Si, Ge, Sn): an EXAFS study†

Trevor Keiber,*[a] Patrick Nast, *[a] Scott Medling,*[a,b] Frank Bridges,*[c] Koichiro Suekuni,*[d] Marcos A. Avila,[e] and Toshiro Takabatake[d]

Received Date
Accepted Date

DOI: 10.1039/xxxxxxxxxx

www.rsc.org/journalname

We report an extended x-ray fine structure (EXAFS) analysis of the type-I clathrates $Ba_8Ga_{16}X_{30}$ (X =Si, Sn) and compare the results with previous works on X = Ge. The distribution of Ga on the three crystallographic cage sites is not random, with the Ga preferentially having X as the nearest neighbor. Our results show that for X = Si, Sn the average pair distances within the cages (Ga-Sn, Ga-Ga, Ga-Si, Sn-Sn) are significantly different than the distances found in x-ray diffraction, with some much shorter bonds and some much longer bonds. These results suggest a substantial buckling of the cages, particularly for $Ba_8Ga_{16}Sn_{30}$. The environment about Ba, extracted from Ba K edge EXAFS, becomes increasingly disordered from Ge to Si to Sn, and for $Ba_8Ga_{16}Sn_{30}$ the nearest Ba neighbor distance is very short, consistent with severe buckling. This buckling contributes to the increased local disorder for $Ba_8Ga_{16}Si_{30}$ and $Ba_8Ga_{16}Sn_{30}$, and provides an explanation for a higher resistivity and a lower ZT than for $Ba_8Ga_{16}Ge_{30}$.

1 Introduction

Clathrates are a promising class of thermoelectric materials made from abundant, earth-friendly elements[1–3]. Clathrates exhibit a rich chemistry with the ability for substitution of many different elements; this allows delicate tuning of both the crystal structure as well as the physical properties. They have been shown to be both chemically and thermally stable at high temperatures, and hold the promise for high temperature applications. A convenient parameter for characterizing the energy conversion potential of thermoelectric materials is the figure of merit ZT defined by $ZT = S^2\,\sigma_e/\kappa$. The desired quantities are a large Seebeck coefficient, S, a moderate electrical conductivity, σ_e and a very low thermal conductivity, κ. Several clathrates have semiconductor-like electric conductivity and glass-like thermal conductivity, which results in a relatively high thermoelectric figure of merit (ZT) with values exceeding 1.3[4].

The thermoelectric properties of the type-I clathrate, $Ba_8Ga_{16}Ge_{30}$, have been investigated extensively in the past[5–12]. More recently the properties of the isostructural materials, $Ba_8Ga_{16}Si_{30}$ and $Ba_8Ga_{16}Sn_{30}$, have been studied;[13–21] surprisingly, although the thermal conductivity is lowest for the Sn compound ($\kappa_{Sn} < \kappa_{Si} < \kappa_{Ge}$[16]), ZT is also lowest (~ 0.6)[22]. ZT for $Ba_8Ga_{16}Ge_{30}$ is highest ((~ 1.3) while ZT of $Ba_8Ga_{16}Si_{30}$ is in between (~ 0.87). The Seebeck coefficient is large for all three compounds but peaks earlier for Sn at approximately 450 K, at 750 K for Ge and even higher for Si. In addition, the electrical resistivity is substantially higher at all temperatures for $Ba_8Ga_{16}Sn_{30}$,[4] which is the dominant factor that leads to a lower ZT for this material. It is likely that differences in disorder account for much of the variation in electrical and thermal transport properties of these systems. Here we use the EXAFS technique[23] to compare the local structure in all three compounds.

Another aspect that has been investigated recently is the distribution of the Ga/Sn or Ga/Si atoms among the three cage sites. Blake *et al.*[7] proposed that Ga-Ga bonds should be avoided; this has been observed in EXAFS studies by Kozina *et al.*[15] for $Ba_8Ga_{16}Sn_{30}$ and recently by Mansour *et al.*[20] for a series of compounds $Ba_8Ga_{16}Ge_{30-x}Si_x$. We include these results in the discussion.

The unit cell of a type-I clathrate is made up of two different size cages, as seen in Fig. 1. The unit cell contains six larger cages of 24 atoms and two smaller cages consisting of 20 atoms. There are two Ba sites; Ba1 is located in the center of the smaller cage, and Ba2 is slightly off center in the larger cage[6,14]. The magnitude and direction of the off center displacement of Ba2 in $Ba_8Ga_{16}Ge_{30}$ was investigated in detail by Jiang *et al.*[6].

[a] *Address, Department of Physics, University of California, Santa Cruz, California 95064, USA.*
[b] *Address, Australian National University, Canberra, Australia.*
[c] *Address, Department of Physics, University of California, Santa Cruz, California 95064, USA; Tel: (831) 459-2893; E-mail: bridges@ucsc.edu.*
[d] *Address, Graduate School of Advanced Sciences of Matter, Hiroshima University, Higashi-Hiroshima 739-8530,*
[e] *Address, CCNH, Universidade Federal do ABC (UFABC), Santo André, SP 09210-580, Brazil.*

There are three unique crystallographic sites in the cage, M1 (6c site), M2 (16i site), and M3 (24k site), that are each occupied by a mixture of Ga and X (X = Si, Ge, Sn).[7,24,25] Due to this mixed occupation of elements among the crystallographic sites, diffraction cannot determine the disorder for each element, it instead provides an average over each of the distinct crystallographic sites. Therefore, to investigate local correlations, we use EXAFS to probe the individual elements and independently determine the bond lengths for the first neighbor and in some cases second neighbors, e.g. for $Ba_8Ga_{16}Sn_{30}$: Ga-Sn, Ga-Ga, Sn-Sn, Ba-Ga pairs.

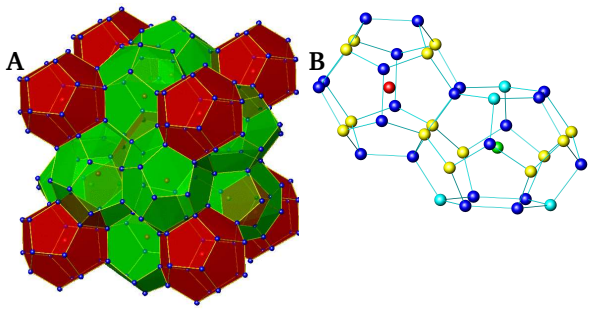

Fig. 1 (Color online) A, the unit cell for a type-I clathrate $Ba_8M_{16}X_{30}$, containing large 24-atom light green cages and smaller 20-atom dark red cages. B, a single cage pair, with rattlers visible in each cage. (M1: light blue, M2: yellow, M3: dark blue.) The Ba rattler in the larger cage, green, is slightly off-center.

Table 1 Pair distances of cage atoms in $Ba_8Ga_{16}X_{30}$ (X = Si, Ge, Sn) from x-ray diffraction[7,13,24].

Pair	$Ba_8Ga_{16}Si_{30}$ 10.5397 Å	$Ba_8Ga_{16}Ge_{30}$ 10.760 Å	$Ba_8Ga_{16}Sn_{30}$ 11.685 Å
M2-M2	2.358	2.496	2.655
M2-M3	2.434	2.441	2.732
M1-M3	2.463	2.503	2.677
M3-M3	2.515	2.541	2.732
Ba1-M2	3.384	3.439	3.731
Ba1-M3	3.464	3.553	3.904
Ba2-M3	3.563	3.612	3.931
Ba2-M1	3.726	3.804	4.131
Ba2-M2	3.909	3.995	4.339
Ba2-M3	4.056	4.157	4.514

2 Experimental Details

The growth and characterization procedures of large single crystals (up to 1 cm) of type-I $Ba_8Ga_{16}Sn_{30}$ and $Ba_8Ga_{16}Ge_{30}$ have been described in previous work.[13] The basic approach is to grow crystals with a self-flux method using excess Ga or Sn, depending on the desired carrier type. High-purity elements are mixed in a glove box, sealed in an evacuated quartz tube, soaked at 490 C, and slowly cooled over 100 hours to 390 C.

To prepare EXAFS samples, the materials were powdered with a mortar and pestle and shaken through a 25 μm sieve. Next a thin layer of powder was brushed onto two pieces of scotch tape, on which the smaller particles preferentially stick. Subsequently, the two pieces of tape were pressed together, forming an encapsulated double layer of particles with sizes $\leq$ 5 μm. The double tape layer was then cut into 2 mm by 16 mm strips which were stacked to obtain an appropriate sample thickness for each absorption edge, such that the edge step height is in the range 0.3-0.9. The samples were mounted in a liquid helium cryostat for temperature dependence studies.

All data were collected on beamline 10-2 at the Stanford Synchrotron Radiation Lightsource (SSRL) in transmission mode. The Ba K edge data were collected using a Si(220) double monochromator, detuned to 80% to reduce harmonics; with a slit height of 0.3 mm, the resulting energy resolution was 7.0 eV. The Sn K-edge data were also collected using a Si(220) double monochromator, but detuned to 50% to reduce harmonics (slit height, 0.3 mm; energy resolution, 4.5 eV). A Si(111) double monochromator, detuned to 50% to reduce harmonics, was used to collect the Ga K-edge data (slit height, 0.5 mm; energy resolution, 2.1 eV). Finally, Due to the low energy of the Si K-edge (1.8 keV), we were unable to collect data for Si, and are limited to using the Ga K-edge to study the Ga-Si substructure in $Ba_8Ga_{16}Si_{30}$.

After collecting the data, we used the RSXAP data reduction package to reduce and fit the data.[26] The reduction follows standard procedures: first a pre-edge background is removed, consistent with the Victoreen formula,[27] and then a spline-fit of the post-edge data provided the average absorption μ_o(E) above the edge. Next, the EXAFS oscillations were extracted, converted to k-space, and fast Fourier transformed (FFT) into r-space using a Gaussian-rounded FT window. The RSFIT program fits the real and imaginary parts of the r-space experimental data to theoretical EXAFS functions generated by FEFF8[28] in order to determine the amplitude, position r, and width, σ, of the pair distribution functions for each atom pair.[28] The Debye-Waller factor σ^2(T) provides a useful measure of both thermal and static disorder for the first few neighbors.

We also determine the parameter ΔE_0 (the difference between the experimental edge energy, defined as the half-height edge energy, and the energy for which k = 0 for the theoretical standards) at low temperature (<100 K), and fix it at that value for the higher temperature fits.

3 Ga K Edge

Ga K-edge k-space data are shown in Fig. 2 for $Ba_8Ga_{16}Si_{30}$ at 6 K; the quality of the data is high out to 15 Å^{-1}. We also have the corresponding Ga edge data for the X = Ge and Sn samples from previous studies.[6,15]

Temperature dependent r-space data are shown in Fig. 3 from 6 to 300 K for $Ba_8Ga_{16}Si_{30}$. We used an FT window of 3.5–14.4 Å^{-1}, Gaussian broadened by σ = 0.3 Å^{-1}. The first peak at approximately 2.0 Å is the sum of several Ga-Si and Ga-Ga pairs due to the three crystallographic sites M1, M2 and M3. This peak is large and has a relatively weak temperature dependence, indicating rigid first neighbor pairs. The presence of a second large peak at 3.4 Å and further neighbors out to 6 Å indicates that the cage structure is reasonably ordered around Ga. The second neighbor

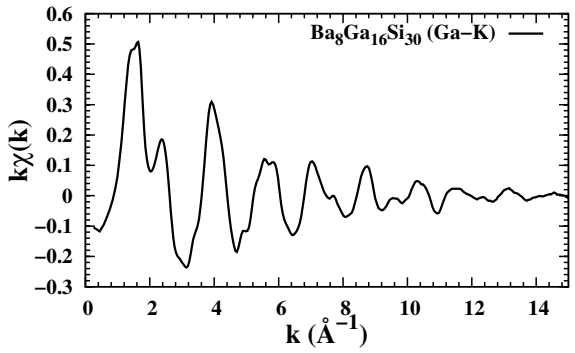

Fig. 2 Ga K edge, k-space data at 6 K for $Ba_8Ga_{16}Si_{30}$.

peak is the sum of many Ga-Ga, Ga-Si and Ga-Ba pairs and has significantly more disorder with temperature. Due to the complexity of this second neighbor peak we will concentrate on the first neighbor.

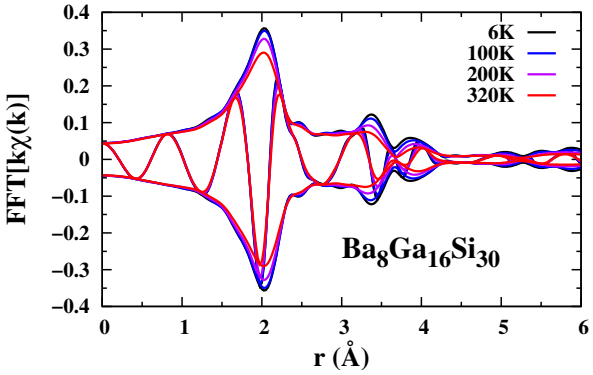

Fig. 3 (Color online) Temperature dependent, Ga K-edge, r-space data for $Ba_8Ga_{16}Si_{30}$. The first neighbor pair is at 2.0 Å; it has a weak temperature dependence and is composed of Ga-Ga and Ga-Si pairs. The second neighbor pair at 3.5 Å is made up of many pairs and decays more rapidly with temperature. Here and in subsequent EXAFS plots, the fast oscillating function is the real part, R, of the FFT while the envelope is $\pm\sqrt{R^2+I^2}$ where I is the imaginary part of the FFT.

In Fig. 4 low temperature Ga edge data collected from previous studies on the system with X = Ge are compared with the current results to observe trends in the type-I clathrate family. The location of the first neighbor peak is shifted between the samples; for the Ge sample, the first neighbor peak (Ga-Ge) is shifted up to 2.2 Å, while for Ga-Sn the peak is located at 2.5 Å, therefore this trend follows closely the increasing atomic radius of the X atoms. The second neighbor peak is located at approximately 3.4 Å for Si. The second peak amplitude, relative to the first peak is largest for X = Ge. The low second neighbor amplitude for the Sn sample indicates significantly more disorder than for the X = Si or Ge samples.

A detailed analysis of the Ga and Ge data for $Ba_8Ga_{16}Ge_{30}$ were presented in Ref.[6] while for $Ba_8Ga_{16}Sn_{30}$ a simple two peak fit was described by Kozina *et al.*[15]. Since the environment around Ga is somewhat more disordered in $Ba_8Ga_{16}Si_{30}$ than in $Ba_8Ga_{16}Ge_{30}$, we follow the method used for $Ba_8Ga_{16}Sn_{30}$.[15] To

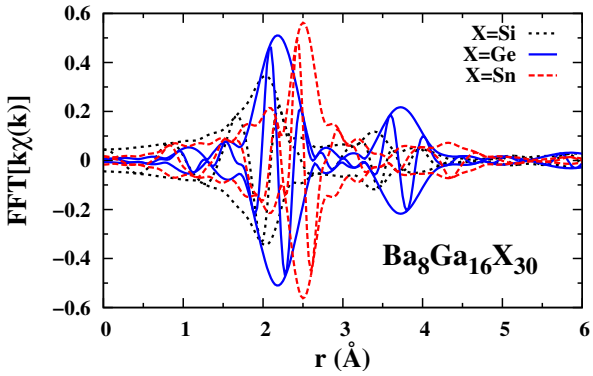

Fig. 4 (Color online) The Ga K edge, r-space data at 10 K are shown for BaGaX (X =Si, Ge, Sn). The position of the first peak shifts with increasing atomic radii or atomic number, from 2 Å for Si, up to 2.5 Å for Sn. The Ge sample is the least disordered. Notice that the second neighbor peak is lowest for the Sn sample (near 4.2 Å), indicating significantly more disorder.

quantify the fraction of Sn neighbors, we fit the first peak in the data to a sum of theoretical functions for the GaâĂŞSi and GaâĂŞGa pairs, with the total coordination number constrained to four total nearest neighbors. Here we use S_o^2 = 1.0 for both pairs.

We started the fit with 75% Ga-Sn (i.e., three Sn neighbors) and 25% Ga-Ga and allowed the ratio to vary along with the width of the pair distribution function and the bond length r of each pair. The fit range was from 1.5 to 3 Å in r space and 3.5 to 14.4 $Å^{-1}$ in k space. Note that the weak GaâĂŞBa1 peak occurs well above 3.3 Å and does not contribute to this first peak. An example of a fit at 6K is shown in Fig. 5. We find that for the best fit, 19% of the nearest neighbors about Ga are Ga, in contrast to the expected 35% from a random distribution. This is in reasonable agreement with Mansour *et al.*[20] who found 22% Ga neighbors in this compound; it is also similar to the result for $Ba_8Ga_{16}Sn_{30}$ for which about 15% of the neighbors are Ga.[15] These fits confirm the visual inspection of Fig. 5, namely, that the GaâĂŞGa bonds make up only a small fraction of the nearest neighbor Ga bonds. The previous EXAFS results[15,20] plus the current results strongly support the Ga-Ga bond avoidance model, first proposed by Blake *et al.*[7]. However, a few Ga-Ga bonds do remain and the number may depend on sample preparation.

In Fig. 6, we compare the bond lengths as a function of temperature from EXAFS and diffraction for $Ba_8Ga_{16}Si_{30}$. Mα-Mβ nearest neighbor distances from x-ray diffraction data are shown as black dashed lines; the EXAFS nearest neighbor distances are (colored) points and have a small temperature dependence. The Ga-Si distance is shorter than the Ga-Ga distance because of the smaller Si atomic radius. For comparison, we have also shown the Si-Si distance in pure Si which is close to the distance for the M2-M2 pair. This suggests that most of the M2-M2 bonds are Si-Si bonds.

4 Sn K Edge

The Sn K edge, r-space data are plotted in Fig. 7 as a function of temperature. There is one peak at 2.5 Å, a sum of Sn-Sn and

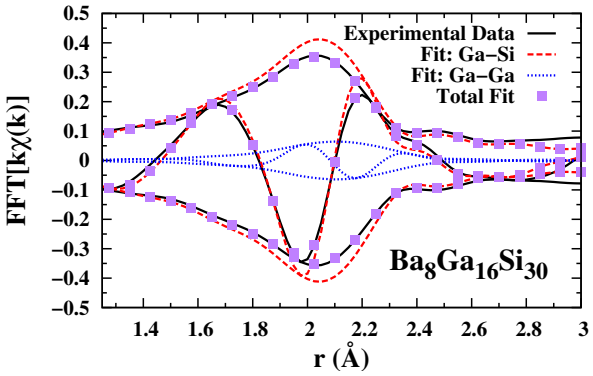

Fig. 5 (Color online) Fit of the Ga K edge data (6 K) with theoretical Ga-Si and Ga-Ga FEFF functions.[28] Note that the Ga-Si peak is dominant and the Ga-Ga peak nearly insignificant. The Ga-Si pair occurs at a shorter r due to a smaller Si atomic radius.

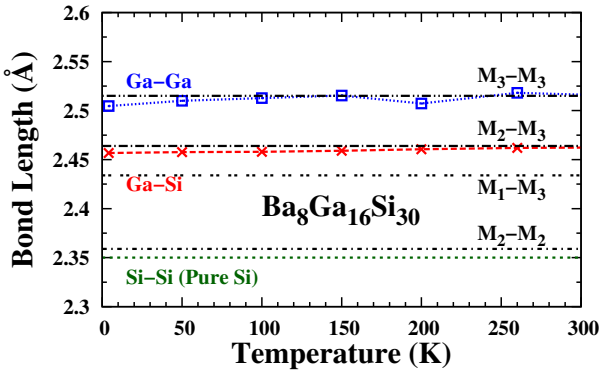

Fig. 6 (Color online) Comparison of bond lengths for $Ba_8Ga_{16}Si_{30}$ determined by EXAFS with crystallographic bond lengths from x-ray diffraction[7], black dashed lines.

Sn-Ga pairs, with no pronounced further neighbor peaks. Our earlier EXAFS study of $Ba_8Ga_{16}Sn_{30}$ at the Ga K edge found the first peak (a sum of Ga-Sn and Ga-Ga pairs) at nearly the same location[15]. There is a moderate temperature dependence for this peak that is greater than for the Ga K edge data, but significantly less than for the Ba K edge (next section). Since further neighbor peaks are small and exhibit minimal temperature dependence they will not be considered for further analysis. It is important to note that for $Ba_8Ga_{16}Ge_{30}$, the corresponding Ge K edge data showed significant second and further neighbor peaks, indicating that the $Ba_8Ga_{16}Ge_{30}$ material is significantly more ordered than $Ba_8Ga_{16}Sn_{30}$.

We fit the peak near 2.5 Å to a sum of Sn-Sn and Sn-Ga theoretical EXAFS functions calculated using FEFF8.[28] This peak is actually the sum of first four pairs, M2-M2, M1-M3, M2-M3 and M3-M3 in the range of 2.66 to 2.77 Å, but because peaks this close together can't be resolved we use a single peak for each type of neighbor. In addition, because of the difference in atomic radii, we expect the Sn-Sn pair distance to be longer. In the fits we allowed the bond distances and the ratio of the number of Sn-Ga and Sn-Sn bonds to vary, with the constraint that the total number of first neighbors forming this peak is 4.0. S_o^2 was set to 1.0. An example of a fit is shown in Fig. 8 at 6 K.

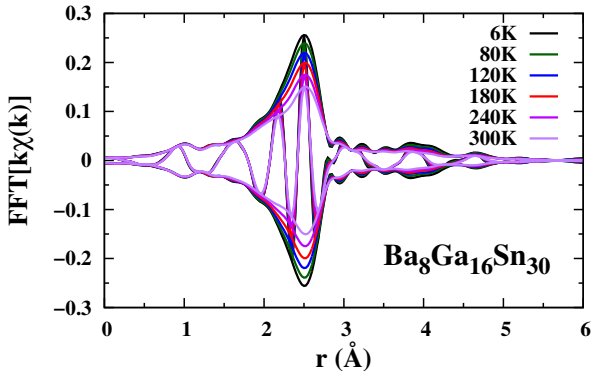

Fig. 7 (Color online) Sn K edge r-space data for $Ba_8Ga_{16}Sn_{30}$ as a function of temperature. The first peak near 2.5 Å is a sum of Sn-Sn and Sn-Ga pairs. FT range; 3.5-15.0 $Å^{-1}$, Gaussian broadened by σ = 0.3 $Å^{-1}$.

EXAFS determines the nearest neighbor distances about each specific atom, while diffraction experiments give an average of the distances between crystallographic sites. The average bond length for the Sn-Ga pair is found to be 2.66 Å while that for Sn-Sn is 2.81 Å. These distances are compared with the diffraction results in Fig. 9; the M-M nearest neighbor distances from room temperature diffraction data are shown as black dashed lines, while EXAFS nearest neighbor pair distances are colored and have a small temperature dependence. The Sn-Ga bond length is close to the shortest of the M-M pairs from x-ray diffraction while the Sn-Sn distance is longer that any of the M-M pairs. Also, the Ga-Ga distance reported by Kozina *et al.*[15] is much shorter than any of the M-M pairs. This combination of very short (2.55 Å) and very long bonds (2.81 Å) in $Ba_8Ga_{16}Sn_{30}$ suggests that buckling may be present—we discuss this in more detail in Sec. 5.1.

The number of Sn-Ga and Sn-Sn bonds are found to be comparable; there are preferentially 2.1 nearest Sn-Ga bonds for every 1.9 Sn-Sn bonds. Note that the ratio of the number of Sn-Ga to Sn-Sn neighbors in a completely random cage filling would be 1.39:2.61; the experimental ratio is > 1 indicating significantly more Sn-Ga neighbors. This is in agreement with the Ga K edge results[15] for which there were few Ga-Ga pairs (and many Ga-Sn pairs).

The Debye-Waller factor, σ^2(T), provides a measure of both static disorder (σ^2_{static}, from strains, off-center displacements, etc.) and thermal disorder that arises from atomic vibrations (phonons), including zero-point-motion contributions. In Fig. 10 we plot σ^2 as a function of temperature for the Ga-Si, Ga-Ge and Ga-Sn pairs as well as for Sn-Sn. σ^2(T) for each pair was fit to a correlated Debye model to extract a static offset (σ^2_{static}) and correlated Debye temperature; values are tabulated in Table 2. The static offset is largest for Ga-Sn which is evidence of more static disorder in this sample, Ga-Si and Ga-Ge have much smaller values. The slope of each curve in Fig. 10 is nearly the same for the Ga-X pairs, indicating very similar effective spring constants (and bond strengths). However the correlated Debye temperatures (See Table 2) vary signifiacntly because we use the pair reduced mass in calculating θ_{cD}. In contrast, the Sn-Sn pair has a

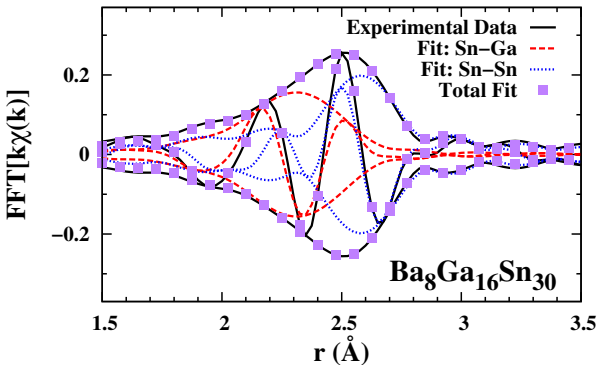

Fig. 8 (Color online) Fit of the Sn K-edge data (6 K) to a sum of theoretical Sn-Sn and Sn-Ga EXAFS functions. Of the four nearest neighbors, on average there are 2.1 nearest Ga neighbors and 1.9 nearest Sn neighbors.

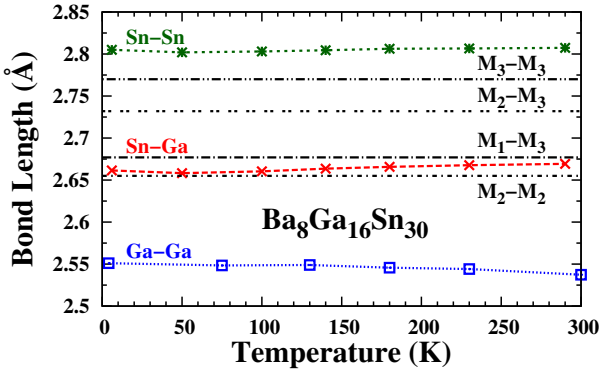

Fig. 9 (Color online) Comparison of bond lengths determined by EXAFS (points) with crystallographic bond lengths from x-ray diffraction (dashed or dotted lines) for $Ba_8Ga_{16}Sn_{30}$. The Sn-Sn bond length is longer while the Ga-Ga bond length is shorter than the bond lengths from diffraction.

larger slope and lower correlated Debye temperature, indicating weaker bonds between the Sn atoms. The largest value for σ^2_{static} occurs for the Ga-Sn pair suggesting significantly increased disorder in $Ba_8Ga_{16}Sn_{30}$; although some of the static disorder arises from different M-M pair distances (see Table 1), the static disorder in $Ba_8Ga_{16}Sn_{30}$ is about 4 times larger than in the other materials.

Table 2 Correlated Debye temperatures, θ_{cD} and static offsets, σ^2_{static}, of selected pairs for $Ba_8Ga_{16}X_{30}$ (X=Ge, Si, Sn).

Pair	θ_{cD} (K)	σ^2_{static} (Å^2)
Ga-Si	527	0.00055
Ga-Ge	415	0.00050
Ga-Sn	345	0.00242
Sn-Sn	269	0.00066

5 Comparison of the Ba Rattler environments in $Ba_8Ga_{16}X_{30}$ (X = Ge, Si, Sn).

There are two Ba sites; Ba1 (25% of Ba) is located in the center of the smaller cage, while Ba2 (75% of Ba) is slightly off center in the larger cage; EXAFS provides a sum over both sites. The

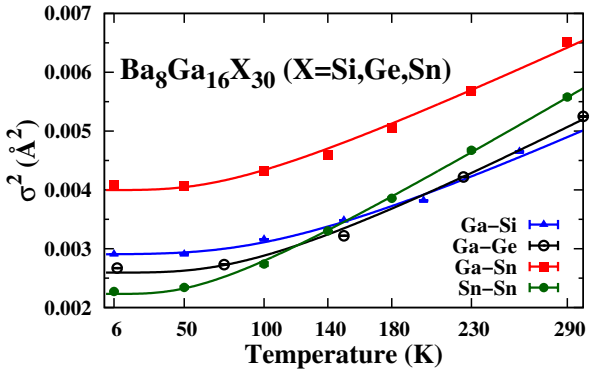

Fig. 10 (Color online) σ^2 as a function of temperature for the Ga-Si, Ga-Ge and Ga-Sn pairs in $Ba_8Ga_{16}X_{30}$ (X = Si, Ge, Sn). Note that the slopes for these three pairs are nearly the same, indicating comparable bond strengths. In contrast, the slope for the Sn-Sn pair is higher and the bond strength is weaker. The data for each pair were fit to a correlated Debye model; note that although the effective spring constants for the Ga-X pairs are about the same, the correlated Debye temperatures, θ_{cD}, are quite different (Table 2) as a result of using a different reduced mass for each pair.

magnitude and direction of the off center displacement of Ba2 in $Ba_8Ga_{16}Ge_{30}$ was the subject of a previous work[6].

Ba K edge EXAFS data were collected for $Ba_8Ga_{16}Si_{30}$ and $Ba_8Ga_{16}Sn_{30}$ out to k = 14 Å^{-1} — see Fig. 11. These data have a much lower amplitude than for $Ba_8Ga_{16}Ge_{30}$,[6] particularly for $Ba_8Ga_{16}Sn_{30}$ for which the EXAFS oscillations die out above $\sim k$ = 10 Å^{-1}, indicating significant disorder.

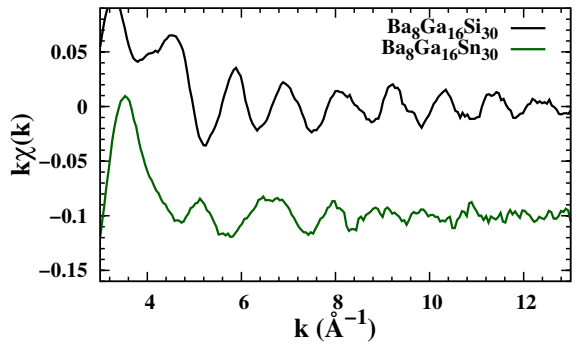

Fig. 11 (Color online) Ba K-edge k-space data for $Ba_8Ga_{16}X_{30}$ X = Si, Sn at 6 K.

We first compare the Ba K edge r-space data for the three clathrate systems $Ba_8Ga_{16}X_{30}$, X = Si, Ge, and Sn, at low temperature — see Fig. 12. This plot shows that the amplitude of the first peak decreases, and hence the neighborhood around Ba becomes more disordered, in the progression from $Ba_8Ga_{16}Ge_{30}$ to $Ba_8Ga_{16}Si_{30}$ to $Ba_8Ga_{16}Sn_{30}$, which is consistent with the decreasing thermal conductivity of these three materials (see Fig. 7 of Ref. 14). However, the large shift of the first peak to lower r (2.6 Å) for $Ba_8Ga_{16}Sn_{30}$ was unexpected, which suggests large distortions are present.

The temperature dependence of the Ba K edge r-space data are plotted in Fig. 13 for $Ba_8Ga_{16}Si_{30}$ and $Ba_8Ga_{16}Sn_{30}$. Because the

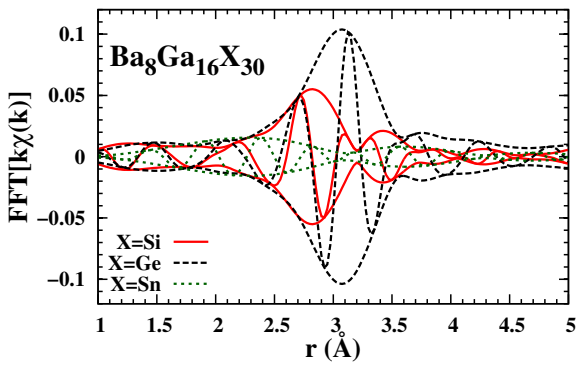

Fig. 12 (Color online) Ba K-edge EXAFS data for the three clathrate compounds $Ba_8Ga_{16}X_{30}$ (X = Si, Ge, Sn). The shift and decrease in amplitude suggests that the Ba "rattler" environment becomes more distorted in the Si and very distorted in the Sn compound. For this comparison at low T we use a wide FT window for X = Si, Ge; 4.8–12.7 Å^{-1}, and a narrower FT range for X = Sn, 5.3–9.2 Å^{-1}, all Gaussian broadened by σ = 0.2 Å^{-1}.

EXAFS oscillations are significantly damped at 300K, we use the following short FT ranges for all temperatures: $Ba_8Ga_{16}Si_{30}$, 5-10 Å^{-1}; $Ba_8Ga_{16}Sn_{30}$, 5.5-9.0 Å^{-1}. The low end of the FT window is constrained by the large width of the Ba edge and some XANES structure near 4 Å^{-1}. Note the very low amplitudes for both samples, indicating significant disorder and likely a decreased number of neighbors.

As show in Fig. 14, for $Ba_8Ga_{16}Si_{30}$ the first peak is near 2.75 Å, while a much smaller peak appears near 3.5 Å; the further neighbor peaks above 4 Å are very small. The relatively low amplitude of the first peak suggests it is likely only from the Ba1 cage which contains just 25% of the Ba atoms. Both peaks have a strong temperature dependence indicating weak bonds between Ba and Ga/Si neighbors. The Ba2 cage with 24 neighbors would lead to a significant peak between 3 and 4 Å if undistorted; the tiny peak near 3.5 Å is likely the remnant of this peak, and the low amplitude indicates significant disorder.

The results for $Ba_8Ga_{16}Sn_{30}$, suggest even more disorder. In this case, although the Ba1 cage distances are longer (3.7 and 3.9 Å), the nearest neighbor peak is near 2.3 Å, with a second small peak near 3.6 Å. Thus, the shortest Ba-(Ga/Sn) distance is at least 1 Å shorter than the crystallographic distances. The very low amplitude of the Ba edge data for $Ba_8Ga_{16}Sn_{30}$, suggest that likely there are very few nearest neighbors, and Ba may be off-center even in the Ba1 cage. If Ba is off-center in both cages, destructive interference between peaks at difference distances can essentially eliminate most of the Ba-(Ga/Sn) peak amplitude.

The Ba K edge data for $Ba_8Ga_{16}Ge_{30}$ were fit by Jiang *et al.*[6] using a highly constrained fit, in which all the bond lengths to atoms within the Ba2 cage could be expressed in terms of a Ba2 off-center displacement, d, while Ba in the Ba1 cage was assumed to be on-center. This required very good signal-to-noise data and lead to an off-center Ba2 displacement of $\sim$ 0.15 Å. For the fit of ($Ba_8Ga_{16}Ge_{30}$), the contributions to the peak near 3.1 Å arises mostly from the two distances in the Ba1 cage plus a contribution from the shorter bonds in the Ba2 cage that arise from the off-center Ba2 position.

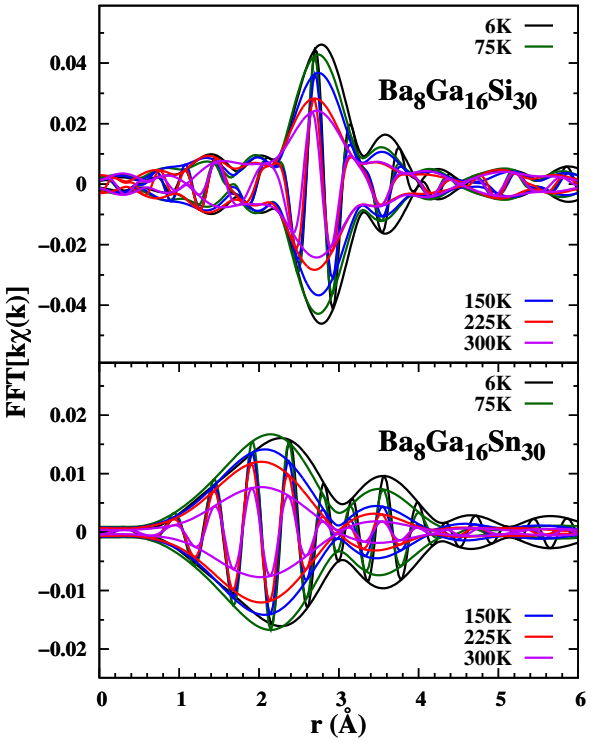

Fig. 13 (Color online) Temperature-dependence of the Ba K-edge r-space data; top panel is $Ba_8Ga_{16}Si_{30}$ with a k-range of 5-10.0 Å^{-1} and bottom is $Ba_8Ga_{16}Sn_{30}$ with a k range of 5.5-9.0 Å^{-1}.

For the $Ba_8Ga_{16}Si_{30}$ sample the average Ba-(Ga/Si) distances for the Ba1 site from x-ray diffraction are 3.38 and 3.46 Å (see Table 1), while all the Ba2-M pairs are 3.56 Å and longer. Thus, to fit the peak near 2.8 Å in Fig. 13 even the Ba1-(Ga/Sn) distances appear too long. However, there is a negative shift of EXAFS peak positions in r-space plots, typically of order –0.2-0.3 Å, but for Ba-Si, closer to –0.5 Å. For Ba2-M peaks, there would have to be a huge off-center displacement of Ba2 in $Ba_8Ga_{16}Si_{30}$, larger than for the Ge compound, to bring one of the Ba2-M peaks down to 2.8 Å; we consider this unreasonable in view of the smaller lattice constant, and assume the peak near 2.8 Å in the experimental data, arises primarily from Ba on the Ba1 site. We treat the peak near 3.5 Å as a small contribution from Ba2-(Ga,Si) pairs. Theoretical EXAFS functions were calculated for Ba-Ga and Ba-Si using FEFF8;[28] these functions were calculated for an average distance of 3.42 Å (Ba1 site), since the distances 3.38 and 3.46 Å cannot be resolved using a short FT range. Although the functions are calculated for the same distance, the position of the theoretical Ba-Si peak is nearly 0.2 Å below that for the Ba-Ga peak, and the real parts of the FT are partially out of phase.

The Ba1 cage consists of eight M2 and twelve M3 sites. If Ga were randomly distributed we would expect the ratio of Si to Ga neighbors to be 30/16 = 1.9; however the analysis of the Ga data indicates Ga-Ga avoidance[15,20] and the Ga distribution is not uniform[8,14,29]. Using the relative distributions reported by Bentien *et al.*[8] and Suekuni *et al.*[14] the ratio of Si to Ga neighbors in the Ba1 cage should be roughly 2.45.

We therefore modeled the first peak as a sum of Ba-Si and Ba-Ga FEFF functions, with the sum of neighbors fixed to 5 (S_o^2 = 1.0; 25% of 20 neighbors = 5), but the ratio of amplitudes unconstrained. We added a longer Ba-Ga peak to model the small peak at 3.5 Å. The positions and widths σ were also allowed to vary. Multiple fits were tried including fits with only one peak for the first peak.

A very good fit was obtained for the 6 K data using the three peak-fit as shown in Fig. 14; the shifts in r (from 3.42 Å) are small for the first neighbor Ba-Si and Ba-Ga pairs – see Table 3 – and the amplitude ratio for the Ba-Si and Ba-Ga is close to 2.5. This is a robust result as we can start the fit at various ratios (1.5, 2, 3 etc.) and the fit result returns to 2.5. The ratio is thus very consistent with other measurements that indicate a non-uniform Ga distribution.[8,14,15] Also, the small values of σ^2 indicate relatively little disorder for the Ba1 peak. However, the small number of neighbors and large value for σ^2, obtained for the small peak near 3.5 Å, indicates significant disorder in the Ba2 cage.

Table 3 Ba K edge fit results at 6 K for $Ba_8Ga_{16}Si_{30}$; bond distance r, number of neighbors, N, and σ^2. Estimated errors: N, 15 %; σ^2, $\pm$ 0.0005 Å^2.

Pair	r (Å)	N	σ^2 (Å^2)
Ba-Si	3.384	3.58	0.0033
Ba-Ga	3.429	1.42	0.0043
Ba-Ga	3.65	2.1	0.0099

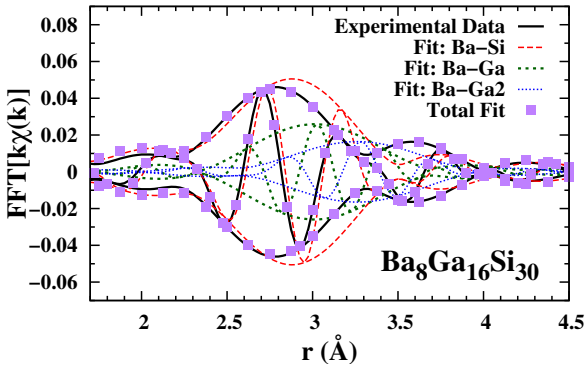

Fig. 14 (Color online) A fit of the Ba K edge data at 6 K, for $Ba_8Ga_{16}Si_{30}$. The experimental data are shown as solid points, with every fifth point plotted for clarity. The total fit is plotted as solid black lines and the three components as dashed or dotted lines. A comparison of the real part, R, of the FT's shows that R for Ba-Si is nearly 90° out of phase with that for the first Ba-Ga, while the two Ba-Ga functions are nearly 180° out of phase. These phase differences are needed to fit the dip near 3.3 Å.

For $Ba_8Ga_{16}Sn_{30}$ the first peak in the Ba K edge data occurs at an even shorter distance (2.3 Å) than for $Ba_8Ga_{16}Si_{30}$ and cannot be fit with theoretical FEFF functions calculated using the crystallographic distances, because the shortest Ba-M distance is about 3.7 Å, in the Ba1 cage. Preliminary fits suggested that the pair distances had to be shortened by roughly 1 Å. A shifted Ba-Ga function was calculated by moving Ba1 off-center such that the Ba-Ga distance was 2.77 Å; this function has a peak at $\sim$ 2.3 Å. For modeling the weak peak near 3.6 Å in Fig. 13, a second FEFF theoretical function was calculated for both Ba-Sn and Ba-Ga pairs at a distance of 3.73 Å, to represent a few Ba-neighbor pairs in either an undistorted Ba1 cage or for a large off-center displacement of Ba in the Ba2 cage.

The best results for the first peak were obtained for a Ba-Ga pair located at 2.74 Å, with $\sim$ 2.0 nearest neighbors. It is substantially broadened with a width σ = 0.135 Å; this large broadening is reasonable as there are likely many different bond lengths. Unfortunately, the amplitude is very low and the data are not good enough for a more complex fit of the first peak.

To fit the further peak at approximately 3.6 Å we again tried various combinations of Ba-Ga and Ba-Sn pairs, with the optimal fit being Ba-Sn. This peak had a significantly reduced amplitude of 0.73 neighbors. It was found to be almost unshifted from the Ba1-M2 pair distance in diffraction; however we could not determine if it was from the Ba1 or Ba2 site. The significantly reduced amplitude is likely due to strong destructive interference effects (in the complex part of the FT) between peaks at many slightly different pair-distances.

These fits show that the disorder about the Ba sites is very large in $Ba_8Ga_{16}Sn_{30}$. The exact nature of the first and second neighbor peaks cannot be uniquely determined due to the low amplitude of the EXAFS oscillations, and significant interference effects. We can say that there are likely approximately two nearest Ga neighbors in the unit cell which are close to Ba; the short distance ($\sim$ 2.74 Å) is close to the sum of the Ba ionic radius (1.43 Å) and the Ga empirical covalent radius (1.26 Å, also roughly half the Ga-Ga bond distance). Thus, these Ba and Ga neighbors are at the position of closest approach.

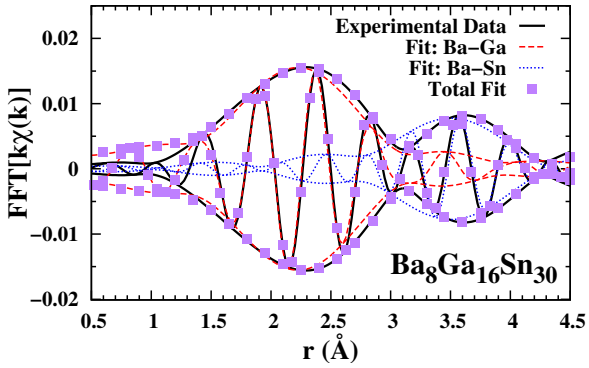

Fig. 15 (Color online) Fit of the Ba K edge data at 6 K for $Ba_8Ga_{16}Sn_{30}$; experimental data are shown as points, but only every sixth point is plotted for clarity. The fits are shown as solid (total fit), dashed (Ba-Ga), and dotted lines (Ba-Sn) . The first neighbor Ba-Ga pair has $\sim$ 2.0 neighbors and is shifted to 2.74 Å, while the second neighbor Ba-Sn pair has 0.73 neighbors with a distance comparable to Ba1-M2 ($\sim$ 3.73 Å).

5.1 Cage buckling

The wide range of bond lengths shown in Fig. 9 for $Ba_8Ga_{16}Sn_{30}$ extend beyond the range of pair M-M distances (Table 1) from x-ray diffraction. To accommodate three long Sn-Sn bonds, a Sn atom would have to be displaced either out of or into the cage

(i.e. away from or towards a Ba atom). Similarly, a very short Ga-Ga bond requires that this Ga pair, connected to several Sn atoms is displaced inwards towards Ba. Two examples are shown in Fig. 16, with the local distortion exaggerated: one shows a Sn atom displaced outwards as a result of three long Sn-Sn bonds, while the other shows a Ga-Ga pair that has moved into the cage to allow the short Ga-Ga bond without stretching the Ga-Sn bonds significantly. This suggests that the cages may be strongly buckled, resulting in some of the Ga/Sn atoms being much closer and others farther from the Ba rattler. The very short Ba-Ga bond length for a few neighbors, found in the Ba K edge analysis supports this model. Significant buckling of the cage will lead to a wide range of slightly different Ba-(Ga/Sn) distances, and in that case destructive interference will greatly decrease the *r*-space amplitude for both cages, as observed.

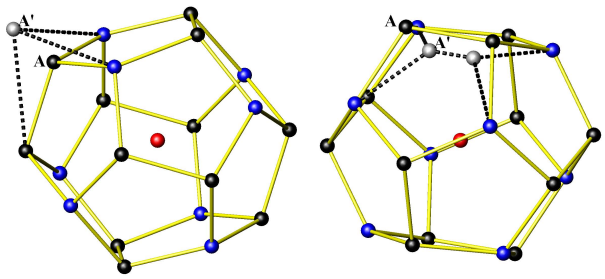

Fig. 16 (Color online) Left: a Sn atom is displaced out of the Ba1 cage to accomodate three long Sn-Sn bonds. Original atom is black (A); displaced atom is grey (A') and dotted lines show the new bonds. Right: a Ga-Ga pair with a short bond length shifts into the cage. Original atom positions are black (A), the displaced atom positions are grey (A'). Again the dotted lines show the new bonds.

There may also be some buckling in $Ba_8Ga_{16}Si_{30}$, as the expected Si-Si distances (from pure Si) are slightly shorter than the M2-M2 distance and significantly shorter than for Ga-Ga. This likely accounts for the increased disorder for the Ba2 site.

A further consequent of buckling is that significant disorder in the cage structures will also lead to charge carrier scattering as well as increased phonon scattering. Such disorder can explain the much lower thermal conductivity[14] and the increased electrical resistivity[22] observed for $Ba_8Ga_{16}Sn_{30}$; the greatly increased electrical resistivity leads to reduced values of *ZT* in spite of the reduced thermal conductivity.

6 Conclusion

For the type-I clathrate $Ba_8Ga_{16}Ge_{30}$, Ga and Ge are neighbors in the periodic table and have have similar covalent radii. Thus, it is difficult to distinguish Ga and Ge in x-ray studies (both in diffraction and EXAFS) and bond lengths Ga-Ge, Ge-Ge etc. are similar. However, when Ge is replaced by either Si or Sn, it becomes easier to differentiate between Ga and Si or Ga and Sn, and because of the difference in covalent radii, a larger difference in bond lengths is anticipated. In EXAFS, the ability to differentiate between Ga and Si or Ga and Sn allows a determination of the number of Ga-Ga bonds, and hence a means of probing the Ga-Ga bond avoidance proposed by Blake *et al.*[7] Bond avoidance was reported for the Sn compound by Kozina *et al.*[15] (15 % of Ga neighbors are Ga), and more recently for the Si compound by Mansour *et al.*[20] (22 % of Ga neighbors are Ga); here we find about 19% of the nearest neighbor bonds are Ga-Ga. Thus, bond avoidance is clearly established and likely is also present in $Ba_8Ga_{16}Ge_{30}$. As shown by Kozina *et al.*[15] there are multiple ways to distribute Ga atoms on the three M sites, and the exact degree of Ga-Ga bond avoidance may depend on sample preparation.

The increased difference in radii leads to a much large difference in local bondlengths, and for $Ba_8Ga_{16}Sn_{30}$, the Sn-Sn bond is longer while the Ga-Ga bond is much shorter than the crystallographic distances. This means that the cages become buckled with some Sn and Ga atoms pushed inwards or outwards from the x-ray diffraction locations. Similar but smaller distortions are present for $Ba_8Ga_{16}Si_{30}$. The presence of significant distortions increases the scattering of charge carriers as well as phonons and leads to increased electrical resistivity, which limits improvements in ZT. For these type-I clathrates it appears that substitution on cage sites may not be useful for thermoelectric applications because of the increased resistivity. Further decreases in thermal conductivity might still be possible by substitutions on the rattler sites (Ba1 and Ba2). If the atom on site 1 were also off-center that would lower the thermal conductivity. If a mixture of atoms (Ca, Sr, Ba, Eu, etc.) were used as rattlers, the avoided crossings[30] could be at several places in *q*-space[31] and that could lead to a further reduction in thermal conductivity.

7 Acknowledgments

This work was supported under NSF grant DMR1005568. Use of the Stanford Synchrotron Radiation Lightsource, SLAC National Accelerator Laboratory, is supported by the U.S. Department of Energy, Office of Science, Office of Basic Energy Sciences under Contract No. DE-AC02-76SF00515. The work at Hiroshima was supported by Grant-in-Aid for Scientific Research from MEXT of Japan, Grant Nos. 18204032, 19051011, and 20102004.

References

1 G. S. Nolas, in *Springer Series in Materials Science* (Springer, ADDRESS, 2014), Vol. 199, pp. 1–326.
2 A. V. Shevelkov and K. Kovnir, Structure and Bonding **139**, 97 (2011).
3 T. Takabatake, K. Suekuni, T. Nakayama, and E. Kaneshita, Rev. Mod. Phys. **86**, 669 (2014).
4 T. Takabatake, in *Nano-Cage Structured Materials: Clathrates*, edited by K. Kumoto and T. Mori (Springer-Verlag, Berlin, 2013), Vol. 182, Chap. 2, pp. 33–49.
5 B. C. Sales, B. C. Chakoumakos, R. Jin, J. R. Thompson, and D. Mandrus, Phys. Rev. B **63**, 245113(1) (2001).
6 Y. Jiang, F. Bridges, M. A. Avila, T. Takabatake, J. Guzman, and G. Kurczveil, Phys. Rev. B **78**, 014111 (2008).
7 N. P. Blake, D. Bryan, S. Latturner, L. Mollnitz, G. D. Stucky, and H. Metiu, Journal of Chemical Physics **114**, 10063 (2001).

8 A. Bentien, E. Nishibori, S. Paschen, and B. B. Iversen, Phys. Rev. B **71**, 144107 (2005).

9 M. A. Avila, K. Suekuni, K. Umeo, H. Fukuoka, S. Yamanaka, and T. Takabatake, Phys. Rev. B **74**, 125109 (2006).

10 T. Mori, S. Goshima, K. Iwamoto, S. Kushibiki, H. Matsumoto, N. Toyota, K. Suekuni, M. A. Avila, T. Takabatake, T. Hasegawa, N. Ogita, and M. Udagawa, Phys. Rev. B **79**, 212301 (2009).

11 Y. Takasu, T. Hasegawa, N. Ogita, M. Udagawa, M. A. Avila, K. Suekuni, and T. Takabatake, Phys. Rev. B **82**, 134302 (2010).

12 K. Iwamoto, S. Kushibiki, H. Honda, S. Kajitani, T. Mori, H. Matsumoto, N. Toyota, K. Suekuni, M. Avila, and T. Takabatake, JPSJ **82**, 024601 (2013).

13 M. A. Avila, K. Suekuni, K. Umeo, H. Fukuoka, S. Yamanaka, and T. Takabatake, Applied Physics Letters **92**, 041901 (2008).

14 K. Suekuni, M. A. Avila, K. Umeo, H. Fukuoka, S. Yamanaka, T. Nakagawa, and T. Takabatake, Phys. Rev. B **77**, 235119 (2008).

15 M. Kozina, F. Bridges, Y. Jiang, M. A. Avila, K. Suekuni, and T. Takabatake, Phys. Rev. B **80**, 212101 (2009).

16 K. Suekuni, T. Tanaka, S. Yamamoto, M. A. Avila, K. Umeo, Y. Takasu, T. Hasegawa, N. Ogita, M. Udagawa, and T. Takabatake, J. Electronic Mater. **38**, 1516 (2009).

17 K. Suekuni, Y. Takasu, T. Hasegawa, N. Ogita, M. Udagawa, M. A. Avila, and T. Takabatake, Phys. Rev. B **81**, 205207 (2010).

18 T. Mori, K. Iwamoto, S. Kushibiki, H. Honda, H. Matsumoto, N. Toyota, M. A. Avila, K. Suekuni, and T. Takabatake, Phys. Rev. Lett. **106**, 15501 (2011).

19 I. Ishii, Y. Suetomi, T. K. Fujita, K. Suekuni, T. Tanaka, T. Takabatake, and T. Suzuki, Phys. Rev. B **85**, 085101 (2012).

20 A. N. Mansour, J. Martin, W. Wong, and G. S. Nolas, J. Phys. Condens. Matter **24**, 485503 (2012), doi:10.1088/0953-8984/24/48/485503.

21 S. Christensen, M. A. Avila, K. Suekuni, R. Piltz, T. Takabatake, and M. Christensen, Dalton Trans. **42**, 14766 (2013).

22 Y. Saiga, K. Suekuni, B. Du, and T. Takabatake, Solid. State Commun. **152**, 1902 (2012).

23 B. K. Teo, *EXAFS: Basic Principles and Data Analysis* (Springer-Verlag, New York, 1986).

24 B. C. Chakoumakos, B. C. Sales, D. G. Mandrus, and G. S. Nolas, Journal of Alloys and Compounds **296**, 80 (2000).

25 B. C. Chakoumakos, B. C. Sales, and D. G. Mandrus, Journal of Alloys and Compounds **322**, 127 (2001).

26 C. H. Booth, *R-Space X-ray Absorption Package, 2010*, 2010, http://lise.lbl.gov/RSXAP/.

27 J. A. Victoreen, J. Appl. Phys. **20**, 1141 (1949).

28 A. L. Ankudinov, B. Ravel, J. J. Rehr, and S. D. Conradson, Phys. Rev. B **58**, 7565 (1998).

29 M. Christensen and B. B. Iversen, Chem. Mater. **19**, 4896 (2007).

30 M. Christensen, A. B. Abrahamsen, N. B. Christensen, F. Juranyl, N. H. Andersen, K. Lefmann, J. Andreasson, and C. R. H. Bahl, Nat. Mat. **7**, 811 (2008), dOI: 10.1038/nmat2273.

31 T. Keiber and F. Bridges, Submitted to Phys. Rev. B (2015).